$\Delta(\Delta S^{\ddagger})$ and $\Delta(\Delta S)$ for the Competing Bond Cleavage Reactions in $(CH_3CN)(ROH)H^+$ [R = CH_3, C_2H_5, C_3H_7, $(CH_3)_2CH$]

Julie A. D. Grabowy and Paul M. Mayer
Department of Chemistry, University of Ottawa, Ottawa, Ontario, Canada

Microcanonical variational transition-state theory was used to determine the entropies of activation for hydrogen-bond cleavage reactions leading to $CH_3CN + ROH_2^+$ in a series of acetonitrile-alcohol proton-bound pairs $(CH_3CN)(ROH)H^+$ (where R = CH_3, CH_3CH_2, $CH_3CH_2CH_2$, and $(CH_3)_2CH$). In each case, the dissociation potential surface was modelled at the MP2/6-31 + G(d) level of theory. The dissociating configurations having the minimum sums-of-states were identified in each case and the resulting entropies of activation were calculated. Combined with previous work on the competing reaction leading to CH_3CNH^+ + ROH, the results permitted the determination of the $\Delta(\Delta S^{\ddagger})$ in each proton-bound pair. For the $(CH_3CN)(CH_3OH)H^+$ and $(CH_3CN)(CH_3CH_2OH)H^+$ proton-bound pairs, the entropies of activation for the two dissociating channels are essentially the same [i.e., $\Delta(\Delta S^{\ddagger}) = 0$], while $\Delta(\Delta S^{\ddagger})$ for the propanol-containing pairs ranged between 40 and 45 J K^{-1} mol^{-1}. The latter non-zero values are due to a combination of the location of the dividing surface in each dissociation and the rapidity with the frequencies of the vanishing vibrational modes go to zero as they are converted to product translations and rotations during the dissociation. (J Am Soc Mass Spectrom 2005, 16, 2039–2044) © 2005 American Society for Mass Spectrometry

The competing dissociation of electrostatically bound molecular pairs forms the basis of the kinetic method [1, 2] for determining a variety of thermochemical parameters such as proton affinities and electron affinities. When considering the dissociation of a proton-bound molecular pair $(A)(B)H^+$ into the products AH^+ + B and BH^+ + A, both the competing energetic and entropic factors must be considered. For simple systems that do not have reverse energy barriers in their dissociation reactions, the locations and characteristics of the effective transition states for the competing pathways determine their relative rate constants. The effective transition-state in each reaction is really a dividing surface along the reaction coordinate that represents a kinetic bottleneck for the dissociation reaction. Identifying this key molecular configuration allows the activation energy, E_a, and entropy, $\Delta S^{\ddagger}$, to be determined. It has been assumed for simple systems that these variational transition states lie at large intracluster separations and thus are product-like. Comparing two such competing reactions results in $\Delta(\Delta S^{\ddagger})$ being similar to $\Delta(\Delta S)$ [2–7], where ΔS is the thermodynamic reaction entropy change for each of the two competing bond scission reactions. This convention has been borne out by several theoretical treatments of the kinetic method. Ervin [8] presented a rigorous analysis of the kinetic method using RRKM theory, placing the effective transition states at the centrifugal barriers to the dissociations. This resulted in $\Delta(\Delta S^{\ddagger})$ always being greater than $\Delta(\Delta S)$ by ~6 J K^{-1} mol^{-1}. Drahos and Vekey [3] also assumed very late transition states in their modeling of the kinetic method (and thus $\Delta(\Delta S^{\ddagger}) = \Delta(\Delta S)$).

In a previous publication [9], we employed microcanonical variational transition-state theory (μ-VTST) to model the unimolecular dissociation of a series of proton-bound acetonitrile-alcohol pairs $(CH_3CN)(ROH)H^+$ (where R = CH_3, CH_3CH_2, $CH_3CH_2CH_2$, and $(CH_3)_2CH$) into CH_3CNH^+ and ROH (Channel A) to arrive at the entropy of activation, $\Delta S^{\ddagger}$. The $\Delta S^{\ddagger}$ was found to decrease from 70 J K^{-1} mol^{-1} for $(CH_3CN)(CH_3OH)H^+$ and 39 J K^{-1} mol^{-1} for $(CH_3CN)(CH_3CH_2OH)H^+$ to 6 and 12 J K^{-1} mol^{-1} for $(CH_3CN)(CH_3CH_2CH_2OH)H^+$ and $(CH_3CN)((CH_3)_2CHOH)H^+$, respectively. This difference in $\Delta S^{\ddagger}$ was not carried over to the ΔS for the four dissociation reactions, which were all similar and between 90–100 J K^{-1} mol^{-1}. In the present study, we have modelled the competing dissociation channel into CH_3CN and ROH_2^+ (Channel B) to determine explicitly $\Delta(\Delta S^{\ddagger})$ and $\Delta(\Delta S)$. As will be seen below, the dynamics of the two channels are quite different necessitating a different computational approach for Channel B than was used for Channel A [9, 10].

Published online October 28, 2005

Address reprint requests to Dr. P. M. Mayer, Department of Chemistry, University of Ottawa, 10 Marie Curie, Ottawa K1N 6N5, ON, Canada. E-mail: pmmayer@uottawa.ca

1044-0305/05/$30.00
doi:10.1016/j.jasms.2005.08.010

Received June 29, 2005
Revised August 18, 2005
Accepted August 20, 2005

Computational Procedures

All ab initio molecular orbital calculations were carried out using the Gaussian 98 suite of programs [11] and geometries were optimized and harmonic vibrational frequencies were calculated, at MP2/6-31+G(d) level of theory. All vibrational frequencies were scaled by the factor of 0.9434 recommended by Scott and Radom [12] before use.

The reaction paths corresponding to Channels A and B in each proton-bound pair do not have formal reaction barriers and so discrete transition states cannot be obtained with ab initio MO calculations. The effective dividing surface for the reactions was located with variational transition-state theory (VTST) according to the following expression [13–16]:

$$k(E) = \frac{\sigma N^{\ddagger}(E,\ E_0,\ R^*)}{h\qquad \rho(E)}$$

where $k(E)$ is the unimolecular rate constant at an ion internal energy, E, σ is the reaction symmetry number, h is Planck's constant, E_0 is the 0 K activation energy, $\rho(E)$ is the reactant ion density of states, and $N^{\ddagger}(E,E_0,R^*)$ is the sum-of-states for the fragmentation bottleneck located at an intra-cluster separation R*. The transition states were located at the intra-cluster separation, R*, that has the lowest sum-of-states and thus the minimum reaction flux. The density and sum-of-states were calculated by the direct count method of Beyer and Swinehart [17]. Over the course of the dissociation reactions, six vibrational modes are converted into product translations and rotations. Of these six modes, the lowest frequency mode corresponded to an intra-cluster torsion mode and was treated as a free rotor in the RRKM calculations [13], whilst the highest frequency mode was the intra-cluster stretching frequency representing the reaction coordinate for the cleavage of the complex. All entropy values (thermodynamic and of activation) were calculated at 600 K.

Results and Discussion

The proton-bound molecular pairs can undergo two competing simple hydrogen bond cleavage reactions:

$$\begin{aligned}(CH_3CN)(ROH)H^+ &\rightarrow CH_3CNH^+ + ROH\\ &\rightarrow CH_3CN + ROH_2^+\end{aligned}$$

In our previous work on Channel A, the dissociation reaction proceeded in a straight-forward manner, with the two separating moieties simply getting farther apart over the course of the reaction [9, 10]. In all of the four optimized proton-bound pairs, the bulk of the positive charge (+0.68) resides on the proton while acetonitrile carries +0.10 charge and the remaining +0.22 being on the alcohol. Breaking the H—O bridging hydrogen bond means that there is a favorable interaction between protonated acetonitrile and the partial negative charge on the hydroxyl group of the alcohol as the two moieties separate. Because of this, an approximate method was used to estimate the vibrational frequencies of the various molecular configurations along the dissociation pathway for each proton-bound pair. This involved assigning the normal modes of $(CH_3CN)(ROH)H^+$ to frequencies of either one of the dissociation products CH_3CNH^+ or ROH (common modes) or to one of the six modes that are converted to translational and rotational degrees of freedom of the products (the vanishing modes) by comparing their calculated atomic displacements. For the common modes, the transition-state frequencies were chosen to be the average of their values in the complex and in the free product and, hence, were the same for every molecular configuration in the dissociation (it was shown that this assumption did not affect the resulting $\Delta S^{\ddagger}$ values [9]. Of the six vanishing modes, the lowest frequency mode was a torsion mode and was treated as a free rotor in the RRKM calculations [13], while the highest frequency mode was the intra-cluster stretching frequency representing the reaction coordinate for the cleavage of the complex. The four remaining frequencies were then scaled according to the following equation [13, 18, 19]:

$$v'(R) = v(R_{eq})e^{-\alpha(R-R_{eq})}$$

where v′(R) is the value of the frequency at an intra-cluster separation R, R_{eq} is the equilibrium hydrogen bond distance and α is an adjustable parameter. This equation is based on the assumption that the four modes vanish exponentially to zero along the reaction coordinate [18, 19]. The parameter was determined by comparing the four vanishing frequencies of each molecular system with those calculated for the optimized CH_3CNH^+—ROH structures having intra-cluster separations of 5.0 and 8.0 Å. The four α values derived for each of the four complexes dissociating by Channel A [9] are relisted in Table 2 for comparison with the Channel B results reported below.

During the dissociation of these proton-bound pairs to form CH_3CN and ROH_2^+ (Channel B), the alcohol rotates with respect to the nitrile to form the configurations shown in Figure 1. The partial charges on the CH_3 and OH_2 groups of protonated methanol at an N—H distance of 16.5 Å from CH_3CN are +0.55 and +0.42, respectively, virtually identical to those found in free $CH_3OH_2^+$. The rotation of the protonated methanol allows a more favorable ion–dipole interaction with the acetonitrile moiety. Similar charge distributions are encountered in the dissociating configurations for the ethanol, *n*- and isopropanol-containing complexes with the charge distribution in the protonated alcohol being identical to that found in the free product. At long range (11.0 Å), the ethanol group has rotated such that the CH_3CH_2 group (+0.57 charge) now lies closest to CH_3CN. The charges are +0.59 and +0.40 on the C_3H_7 and OH_2 groups of protonated *n*-propanol (at 12.0 Å) while those on isopropanol (at 12.5 Å) are +0.58 and +0.42, respectively. All of these configurations can be

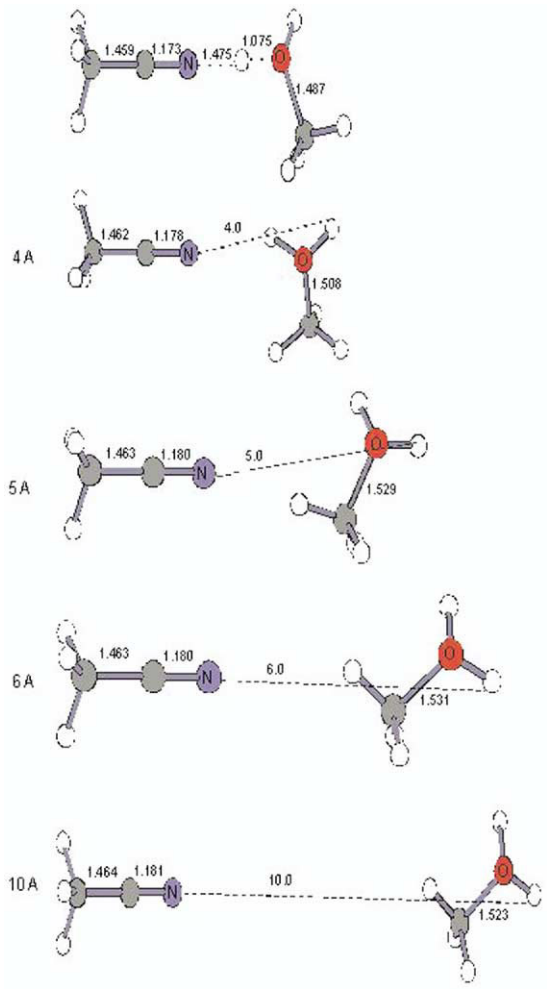

Figure 1. MP2/6-31 + G(d) optimized geometries of the $(CH_3CN)(CH_3OH)H^+$ proton-bound pair at a series of $CH_3CN—H^+O(H)CH_3$ bond distances.

summarized as ion–dipole complexes between CH_3CN and the protonated alcohol.

Since the conformation of the system in Channel B changes over the course of the dissociation, it was no longer possible to employ the method outlined above for estimating the vibrational frequencies for molecular configurations along the reaction coordinate. Instead, full geometry optimizations (and frequency analyses) were required for all structures along the dissociation pathways. The N—H bond was stretched in 0.5 Å increments, held fixed at each point and the rest of the geometric parameters optimized before performing vibrational frequency analyses. Geometry optimizations were done on each structure beginning with the equilibrium geometry and ending with the configuration at an N—H bond separation of 17 Å for the $(CH_3CN)(CH_3OH)H^+$ and 13 Å for the ethanol, *n*- and isopropanol-containing proton-bound pairs. The calculated vibrational frequencies were then used to determine the configuration representing the minimum in the sum-of-states (the effective transition-state, Table 1) and, therefore, $\Delta S^{\ddagger}$ (Table 2). Due to the rotation of the alcohol moiety, the fixed N—H bond distances presented above were not the smallest geometrical distances between the two separating moieties. Therefore, the minimum distances (between acetonitrile and the alkyl portion of ROH) were used in the subsequent analysis.

The effective transition states for dissociation for Channel B in these four proton-bound pairs were found to lie at intra-cluster separations (R*) similar to those observed for Channel A (Table 2); 3.7, 3.5, 3.4, and 3.4 Å for $(CH_3CN)(CH_3OH)H^+$, $(CH_3CN)(CH_3CH_2OH)H^+$, $(CH_3CN)(CH_3CH_2CH_2OH)H^+$, and $(CH_3CN)((CH_3)_2CHOH)H^+$, respectively. All the dissociation reactions via Channel B had clear minima in the sum-of-states at the R* values listed in Table 2 except for $(CH_3CN)(CH_3OH)H^+$. For this pair, the R* was taken at a point where $\Delta S^{\ddagger}$ had converged (Figure 2). These effective transition states indicate that the dividing surface for these reactions is situated near the products. Phase Space Theory (PST), employing an ion/polarizable atom model [20], places the centrifugal barriers for these reactions at around 12 Å.

The $\Delta S^{\ddagger}$ for the dissociation of $(CH_3CN)(CH_3OH)H^+$ via Channel B is 67 J K^{-1} mol^{-1}, which is within error to that found for Channel A (Table 2). A similar result is obtained for $(CH_3CN)(CH_3CH_2OH)H^+$. As a result, the difference in $\Delta S^{\ddagger}$ for the two competing dissociation channels, $\Delta(\Delta S^{\ddagger})$, for both of these systems is approximately zero. Comparable Channel B $\Delta S^{\ddagger}$ values were determined for $(CH_3CN)(CH_3CH_2CH_2OH)H^+$ and $(CH_3CN)((CH_3)_2CHOH)H^+$, 51 and 54 J K^{-1} mol^{-1}, respectively; while these Channel B values are similar to those obtained for $(CH_3CN)(CH_3OH)H^+$ and $(CH_3CN)(CH_3CH_2OH)H^+$ they are significantly larger than those obtained for Channel A (Table 2). So, according to the present treatment, $\Delta(\Delta S^{\ddagger})$ for the competing dissociations of the two propanol-containing proton-bound pairs are not zero. It is worthwhile determining the possible impact of using two different computational methods for Channels A and B. For example, if we look at Channel A for $(CH_3CN)(CH_3OH)H^+$, the approximate method based on fully optimized geometries at R* = 5 and 8 Å predicted α-values (see Table 2) that led to a transition-state located at 7 Å. If we optimize the structure at 7 Å, the resulting vibrational frequencies give rise to similar α-values (0.49, 0.46, 0.21, 0.18 $Å^{-1}$), and so this structure would also be the transition-state in the fully optimized method, giving rise to a similar $\Delta S^{\ddagger}$. Obviously, agreement between the two methods is better if the transition-state is near to the two points optimized in the approximate method.

Two factors are at play in determining $\Delta S^{\ddagger}$ for these dissociation reactions. One is the location of the dividing surface and the other is how "fast" the four vanishing modes go to zero over the course of the dissociation (as exemplified by the α values that can be derived from eq 2). A dissociation in which the vibrational frequencies go to zero rapidly with increasing separation of the products, and for which the dividing surface lies close

Table 1. Vibrational frequencies used to determine $\Delta S^{\ddagger}$ for the dissociation of the proton-bound pairs into CH_3CN and ROH_2^+. Intracluster separations at the transition state are shown in parentheses

	Harmonic vibrational frequencies (cm^{-1})
$(CH_3CN)(CH_3OH)H^+$	67, 80, 129, 147, 260, 329, 331, 517, 882, 908, 964, 1013, 1015, 1098, 1160, 1290, 1374, 1417, 1417, 1419, 1451, 1454, 1665, 1943, 2155, 2943, 2983, 3039, 3040, 3103, 3117, 3470
TS (13.7 Å)	8, 14, 14, 15, 253, 313, 313, 727, 791, 885, 909, 1020, 1020, 1128, 1241, 1379, 1422, 1436, 1436, 1439, 1441, 1637, 2090, 2942, 2991, 3032, 3032, 3126, 3133, 3364, 3453
$(CH_3CN)(CH_3CH_2OH)H^+$	36, 51, 88, 125, 207, 251, 328, 329, 408, 512, 783, 790, 900, 950, 970, 1014, 1015, 1066, 1157, 1223, 1268, 1369, 1418, 1419, 1446, 1456, 1473, 1664, 2144, 2159, 2937, 2943, 2991, 3019, 3039, 3039, 3040, 3073, 3455
TS (7.5 Å)	11, 17, 20, 20, 169, 259, 314, 314, 356, 675, 738, 775, 884, 901, 934, 1020, 1020, 1092, 1195, 1273, 1340, 1380, 1388, 1435, 1435, 1440, 1452, 1463, 1635, 2091, 2933, 2943, 3012, 3018, 3033, 3033, 3034, 3095, 3364, 3459
$(CH_3CN)(CH_3CH_2CH_2OH)H^+$	33, 40, 86, 111, 121, 186, 225, 286, 328, 329, 434, 511, 746, 825, 864, 893, 903, 969, 1013, 1015, 1017, 1087, 1158, 1204, 1247, 1279, 1310, 1374, 1375, 1395, 1419, 1419, 1456, 1461, 1466, 1472, 1663, 2146, 2193, 2926, 2936, 2943, 2979, 2989, 3019, 3032, 3040, 3040, 3063, 3452
TS (7.4 Å)	6, 12, 20, 20, 119, 187, 221, 241, 314, 314, 395, 705, 721, 755, 862, 881, 884, 950, 1002, 1020, 1020, 1126, 1164, 1224, 1277, 1294, 1358, 1380, 1394, 1435, 1435, 1454, 1459, 1460, 1471, 1616, 2091, 2932, 2941, 2943, 2993, 2997, 3028, 3033, 3033, 3039, 3082, 3357, 3455
$(CH_3CN)((CH_3)_2CHOH)H^+$	36, 47, 89, 116, 197, 219, 265, 329, 330, 352, 388, 449, 510, 706, 875, 898, 916, 920, 954, 1014, 1015, 1064, 1109, 1176, 1235, 1308, 1355, 1374, 1395, 1396, 1419, 1420, 1438, 1446, 1456, 1464, 1671, 2141, 2348, 2930, 2938, 2943, 2980, 3015, 3026, 3031, 3036, 3039, 3040, 3445
TS (8.4 Å)	8, 11, 19, 19, 161, 226, 264, 314, 314, 343, 350, 424, 590, 731, 854, 884, 889, 914, 922, 1020, 1020, 1073, 1152, 1192, 1302, 1346, 1380, 1387, 1395, 1430, 1436, 1436, 1441, 1453, 1460, 1619, 2091, 2928, 2932, 2943, 3010, 3013, 3019, 3031, 3033, 3033, 3039, 3357, 3459

to the products will have a large $\Delta S^{\ddagger}$ value. If the dividing surface of this system moves towards the reactant, the $\Delta S^{\ddagger}$ value will drop since the values of the four vanishing vibrational frequencies will become more reactant-like. The α values for each dissociation reaction and the location of the variational transition-state, R*, are listed in Table 2. When the transition-state frequencies for the four vanishing modes for each channel in $(CH_3CN)(CH_3OH)H^+$ and $(CH_3CN)(CH_3CH_2OH)H^+$ are compared to their respective val-

Table 2. Dividing surface location, R*, α parameters, $\Delta S^{\ddagger}$ and ΔS for Channels A and B[a]

	$CH_3CNH^+ + ROH$ (A)				$CH_3CN + ROH_2^+$ (B)					
$(CH_3CN)(ROH)H^+$	α ($Å^{-1}$)	R*	$\Delta S^{\ddagger}$[b]	ΔS[c]	α ($Å^{-1}$)	R*	$\Delta S^{\ddagger}$[b]	ΔS[c]	$\Delta(\Delta S)^{\ddagger}$	$\Delta(\Delta S)$
R = CH_3	0.46	7.0	70 ± 8	92	0.17	13.7	67	90	3 ± 11	2
	0.44				0.14					
	0.20				0.18					
	0.20				0.19					
R = CH_3CH_2	0.27	6.5	39 ± 4	103	0.20	7.5	43	100	−4 ± 7	3
	0.31				0.19					
	0.25				0.25					
	0.25				0.30					
R = $CH_3CH_2CH_2$	0.13	8.5	6	94	0.29	7.4	51	91	−45 ± 6	3
	0.09				0.20					
	0.03				0.25					
	0.08				0.29					
R = $(CH_3)_2CH$	0.13	7.5	12 ± 4	100	0.23	8.4	54	101	−42 ± 7	−1
	0.17				0.22					
	0.04				0.23					
	0.09				0.27					

[a] in J K^{-1} mol^{-1}.
[b] ± 3 J K^{-1} mol^{-1} unless otherwise stated. For Channel A, ± 3 J K^{-1} mol^{-1} comes from the averaging of the α-values obtained from the optimized structures at 5 and 8 A along the reaction coordinate [9]. The remainder of the uncertainty is due to the decrease in R* with increasing internal energy. For Channel B, the error is due only to the decrease in R* with increasing internal energy, which was no more than ± 3 J K^{-1} mol^{-1} in each case.
[c] Calculated using eq 7–9 in reference [9].

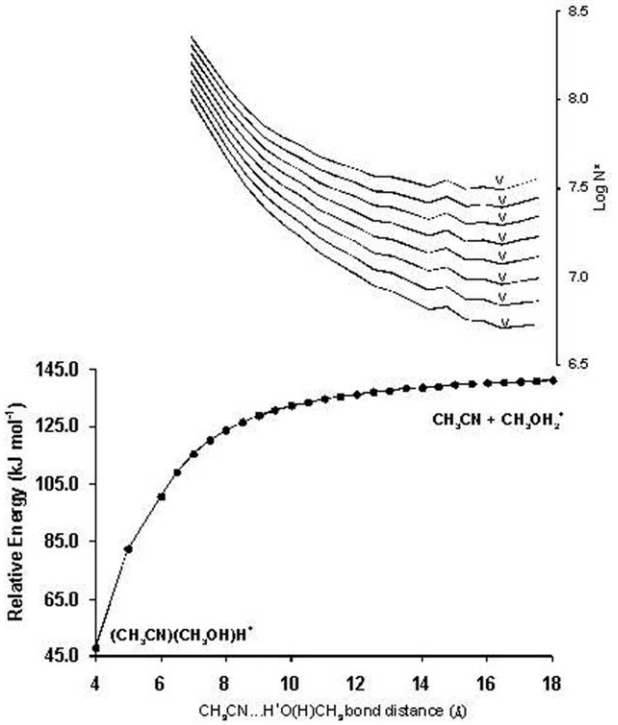

Figure 2. Plot of the relative energy versus $CH_3CN—H^+$ $O(H)CH_3$ bond distance in the $(CH_3CN)(CH_3OH)H^+$ complex at the MP2/6-31 + G(d) level of theory. Superimposed on the figure is the calculated sum-of-states, log $N^‡$, as a function of R at various internal energies. The location of the transition-state is denoted with V.

ues in the equilibrium structures, the average deviations are similar, resulting in $\Delta(\Delta S^‡) \approx 0$. For example, in $(CH_3CN)(CH_3OH)H^+$, R* for Channel B is located at 13.7 Å, while that for Channel A is 7.0 Å. The resulting α values for the four vanishing modes produce transition-state vibrational frequencies that differ from the equilibrium values (differences of 4, 5, 35, and 40 for Channel A and 8, 14, 14, and 15 for Channel B) with similar average deviations of 17 and 13 cm^{-1}, for Channels A and B, respectively. For $(CH_3CN)(CH_3CH_2CH_2OH)H^+$, the combination of the location of the dividing surface and the α values result in quite different average deviations in the transition-state frequencies for the two competing channels in each case: 57 cm^{-1} for Channel A and 22 cm^{-1} for Channel B. A similar result is obtained for $(CH_3CN)[(CH_3)_2CHOH]H^+$. Thus, $\Delta(\Delta S^‡)$ is not zero for these two proton-bound molecular pairs. Thermodynamic entropy changes for the dissociations of $(CH_3CN)(CH_3OH)H^+$, $(CH_3CN)(CH_3CH_2OH)H^+$, $(CH_3CN)(CH_3CH_2CH_2OH)H^+$, and $(CH_3CN)((CH_3)_2CHOH)H^+$ are also listed in Table 2. As expected for simple molecular systems, the entropy changes for Channels A and B are nearly the same in each case and $\Delta(\Delta S)$ are zero.

Unfortunately, a full kinetic method analysis of these proton-bound pairs is not practical as Channels A and B are both observed in only two cases, R = C_2H_5 and C_3H_7. The more favorable entropy change in the lower energy Channel B reactions (R = C_3H_7 and $(CH_3)_2CH$) would lead to a greater observed ratio for $[ROH_2^+]/[CH_3CNH^+]$ in these two cases than if $\Delta(\Delta S^‡) = 0$. Quantitatively, the $\Delta(\Delta S^‡)$ of ~45 J K^{-1} mol^{-1} for the two propanol containing pairs, if ignored, would result in a potential discrepancy in ΔPA of 5.4 RT_{eff}.

Conclusions

The entropies of activation for the dissociation of a series of acetonitrile-alcohol proton-bound pairs, $(CH_3CN)(CH_3OH)H^+$, $(CH_3CN)(CH_3CH_2OH)H^+$, $(CH_3CN)(CH_3CH_2CH_2OH)H^+$, and $(CH_3CN)[(CH_3)_2CHOH]H^+$, were compared for two dissociation pathways (CH_3CNH^+ + ROH and CH_3CN + ROH_2^+) using microcanonical variational transition-state theory. The dissociation of the proton-bound pairs via Channel A to form CH_3CNH^+ and neutral alcohol occurred by simple bond dissociation in which the two departing fragments simply got farther apart. Over the course of dissociation by Channel B, the departing protonated alcohol moiety rotates to produce a more favorable interaction with the dipole of the neutral acetonitrile. The absolute $\Delta S^‡$ values for each dissociation pathway were found to be determined by the combination of the location of the dividing surface and the rapidity with which the four key vanishing modes in each dissociation tended to zero as a function of increasing separation of the products.

Acknowledgments

PMM thanks the Natural Sciences and Engineering Research Council of Canada for continuing financial support.

References

1. McLuckey, S. A.; Cameron, D.; Cooks, R. G. Proton Affinities from Dissociations of Proton-Bound Dimers. *J. Am. Chem. Soc.* **1981,** *130,* 1313–1317.
2. Zheng, X.; Cooks, R. G. Thermochemical Determinations by the Kinetic Method with Direct Entropy Correction. *J. Phys. Chem. A* **2002,** *106,* 9939–9946.
3. Drahos, L.; Vekey, K. Entropy Evaluation Using the Kinetic Method: Is It Feasible? *J. Mass Spectrom.* **2003,** *38,* 1025–1042.
4. Cheng, X.; Wu, Z.; Fenselau, C. Collision Energy Dependence of Proton-Bound Dimer Dissociation: Entropy Effects, Proton Affinities, and Intramolecular Hydrogen-Bonding in Protonated Peptides. *J. Am. Chem. Soc.* **1993,** *115,* 4844–4848.
5. Wu, Z.; Fenselau, C. Gas-Phase Basicities and Proton Affinities of Lysine and Histidine Measured from the Dissociation of Proton-Bound Dimers. *Rapid Commun. Mass Spectrom.* **1994,** *8,* 777.
6. Cerda, B. A.; Hoyau, S.; Ohanessian, G.; Wesdemiotis, C. Binding to Cyclic and Linear Dipeptides. Bond Energies, Entropies of Na^+ Complexation and Attachment Sites from the Dissociation of Na^+-Bond Heterodimers and Ab Initio Calculations. *J. Am. Chem. Soc.* **1998,** *120,* 2437–2448.
7. Cerda, B. A.; Wesdemiotis, C. Gas Phase Copper (I) Ion Affinities of Valine, Lysine, and Arginine Based on the Disso-

ciation of Cu^+-Bound Heterodimers at Varying Internal Energies. *Int. J. Mass Spectrom.* **1999**, *185/186/187*, 107–116.
8. Ervin, K. M. Microcanonical Analysis of the Kinetic Method. The Meaning of the "Apparent Entropy". *J. Am. Soc. Mass Spectrom.* **2002,** *13,* 435–452.
9. Grabowy, J. A. D.; Mayer, P. M. Entropy Changes in the Dissociation of Proton-Bound Complexes: A Variational RRKM Study. *J. Phys. Chem. A* **2004,** *108,* 9726–9732.
10. Grabowy, J. A. D.; Mayer, P. M. Entropy Changes in the Dissociation of Proton-Bound Complexes: A Variational RRKM Study (Erratum). *J. Phys. Chem. A* **2005,** *109,* 5243–5244.
11. Frisch, M. J.; Trucks, G. W.; Schlegel, H. B.; Scuseria, G. E.; Robb, M. A.; Cheeseman, J. R.; Zakrzewski, V. G.; Montgomery, J. A.; Stratmann, R. E.; Burant, J. C.; Dapprich, S.; Millam, J. M.; Daniels, A. D.; Kudin, K. N.; Strain, M. C.; Farkas, O.; Tomasi, J.; Barone, V.; Cossi, M.; Cammi, R.; Mennucci, B.; Pomelli, C.; Adamo, C.; Clifford, S.; Ochterski, J.; Petersson, G. A.; Ayala, P. Y.; Cui, Q.; Morokuma, K.; Malick, D. K.; Rabuck, A. D.; Raghavachari, K.; Foresman, J. B.; Cioslowski, J.; Ortiz, J. V.; Stefanov, B. B.; Liu, G.; Liashenko, A.; Piskorz, P.; Komaromi, I.; Gomperts, R.; Martin, R. L.; Fox, D. J.; Keith, T.; Al-Laham, M. A.; Peng, C. Y.; Nanayakkara, A.; Gonzalez, C.; Challacombe, M.; Gill, P. M. W.; Johnson, B.; Chen, W.; Wong, M. W.; Andres, J. L.; Gonzalez, C.; Head-Gordon, M.; Replogle, E. S.; Pople, J. A. *Gaussian 98 Rev. A7*; Gaussian Inc.: Pittsburgh PA, 1998.
12. Scott, A. P.; Radom, L. Harmonic Vibrational Frequencies: An Evaluation of Hartree-Fock, Moller-Plesset, Quadratic Configuration Interaction, Density Functional Theory, and Semi-Empirical Scale Factors. *J. Phys. Chem.* **1996,** *100,* 16502–16513.
13. Baer, T.; Hase, W. L. Unimolecular Reaction Dynamics, Theory, and Experiments; Oxford University Press: New York, 1996; pp 439–442
14. Pechukas, P. Transition State Theory. *Annu. Rev. Phys. Chem.* **1981,** *32,* 159–177.
15. Truhlar, D. G.; Garrett, B. C. Variational Transition-State Theory. *Acc. Chem. Res.* **1980,** *13,* 440–448.
16. Lifshitz, C.; Louage, F.; Aviyente, V.; Song, K. Transition-State Switchings for Single Potential Well Ionic Dissociations. *J. Phys. Chem.* **1991,** *95,* 9298–9302.
17. Beyer, T.; Swinehart, D. R. Number of Multiply-Restricted Partitions [A1] (Algorithm 448). *ACM Commun.* **1973,** *16,* 379.
18. Hase, W. L. Theoretical Critical Configuration for Ethane Decomposition and Methyl Radical Recombination. *J. Chem. Phys.* **1972,** *57,* 730–733.
19. Quack, M.; Troe, J. Specific Rate Constants of Unimolecular Processes. J. Ber. Bunsenges. Phys. Chem. **1974,** *78,* 240–252.
20. Gridelet, E.; Lorquet, J. C.; Levh, J. Role of Angular Momentum Conservation in Unimolecular Translational Energy Release: Validity of the Orbiting Transition State Theory. *J. Chem. Phys.* **2005,** *122,* 094106.